ARTICLE IN PRESS

Available online at www.sciencedirect.com

ScienceDirect

Advances in Space Research xxx (xxxx) xxx

ADVANCES IN SPACE RESEARCH (a COSPAR publication)

www.elsevier.com/locate/asr

Spectral features of ground-level enhancement and Forbush decrease in solar cycle 25

B. Sargsyan, A. Chilingarian *

A. I. Alikhanyan National Science Laboratory (Yerevan Physics Institute) Yerevan, Armenia Alikhanyan Brothers 2, Yerevan 36, AM00036, Armenia

Received 29 January 2026; received in revised form 14 April 2026; accepted 15 April 2026

Abstract

After a very calm 24th solar activity cycle, the 25th cycle has already seen several interesting events. A Ground Level Enhancement (GLE 77) was observed on 11 November 2025 following an X5.1-class solar flare. A strong Forbush decrease (FD) occurred on 19–20 January 2026 during one of the most intense geomagnetic storms of Solar Cycle 25. Events were recorded coherently by the global neutron monitor (NM) network and by SEVAN detectors at multiple altitudes. Using SEVAN's light-spectrometric capabilities, we reconstruct energy-dependent spectra of "missing" neutrons and muons during the FD and compare them with corresponding spectra measured during GLE 77. The analysis shows that FD and GLE signatures are intrinsically asymmetric: FDs selectively suppress the pre-existing galactic cosmic-ray population, whereas GLEs introduce an additional, harder particle component. Neutron and muon channels exhibit markedly different spectral behavior, particularly at higher deposited energies, reflecting their sensitivity to different primary-energy ranges. These results show that combined NM–SEVAN observations provide robust, complementary diagnostics of rigidity-dependent cosmic-ray modulation during extreme heliospheric disturbances.

Keywords: Forbush decrease; Ground level enhancement; Neutron monitors; SEVAN detectors

1. Introduction

Ground-level Enhancements (GLEs) are high-energy events in which solar protons reach energies sufficient to generate secondary cascades detectable by ground-based detectors (Shea and Smart, 2012). GLEs are the highest-energy manifestation of solar energetic protons (SEP; Reames, 2013); 77 GLEs have been officially registered, predominantly associated with major eruptive flares and ICME-driven shocks (Bütikofer and Flückiger, 2015).

The particle fluxes measured at Earth's surface show depletions (called Forbush Decreases – FDs) caused by disturbances in near-Earth magnetic structures in response to interplanetary shocks and ICMEs (Maricic et al., 2014). FDs are the most common and easiest to detect phenomenon of solar modulation of galactic cosmic rays. More than 80 years ago, Scott Forbush was the first to connect these depletions in the cosmic radiation (CR) flux to solar eruptions (Forbush, 1954).

FDs and GLEs are two distinct types of solar–terrestrial interactions. FDs result from the suppression of galactic cosmic rays (GCRs) by interplanetary magnetic structures associated with coronal mass ejections, while GLEs occur when high-energy solar protons are injected into the near-Earth environment. Although both phenomena are routinely detected by neutron monitors (NMs), and the energy spectrum of solar protons has been inferred using

* Corresponding author.
E-mail address: chili@aragats.am (A. Chilingarian).

https://doi.org/10.1016/j.asr.2026.04.068

Please cite this article as: B. Sargsyan and A. Chilingarian, Spectral features of ground-level enhancement and Forbush decrease in solar cycle 25, Advances in Space Research, https://doi.org/10.1016/j.asr.2026.04.068

the global NMs network (Mishev and Usoskin, 2016; Tylka and Dietrich, 2009), the high-energy tail and various secondary particle channels remain insufficiently explored.

The SEVAN detector concept (Chilingarian et al., 2018), which combines neutron- and muon-sensitive channels at a single site, offers a more detailed view of cosmic-ray modulation. While neutron monitors mainly detect lower-rigidity primaries, muons indicate much higher primary energies. This work uses simultaneous NM and SEVAN observations of the November 11, 2025, GLE and the January 2026 FD to reconstruct energy-dependent spectra and compare them, emphasizing significant spectral differences rather than acceleration modeling.

2. GLE 77 on 11 November 2025: the second-largest GLE in 20 years after GLE 69 on 20 January 2005

The GLE 77 occurred on 11 November 2025 in association with an X5.1-class solar flare, which reached its soft X-ray maximum at 10:04 UT, as recorded by Geostationary Operational Environmental Satellite (GOES) X-ray sensors. High-energy proton channels on GOES-18 (Kress et al., 2020) showed a rapid intensity increase within several minutes after the flare peak, indicating prompt acceleration and rapid interplanetary transport of relativistic solar protons to 1 AU. Neutron monitors (NMs) and the SEVAN network detected the onset of GLE 77 at 10:12–10:14 UT. The peak response varied strongly among stations, reflecting their differing geomagnetic cutoff rigidities. In contrast to large polar events, the response at mid-latitude stations was modest, indicating a limited flux of very high-rigidity particles.

Fig. 1 shows the time series of neutron flux increases, measured in standard deviations (σ) relative to the pre-event baseline. We compare GLE 69 and GLE 77 using significance analysis on Aragats NM (ArNM), Nor Amberd NM (NANM), and the Aragats Solar Neutron Telescope (ASNT) 5 cm scintillator channel, which is mostly sensitive to muons. The particle selectivity of the SEVAN coincidence channels is summarized in Table 1 of (Chilingarian et al., 2024). For each detector, the baseline mean and standard deviation were calculated from a 1-hour reference period. Both GLE 69 and GLE 77 are clearly detected in 5-minute significance series. GLE 69 exhibits a very strong ArNM response, reaching 11.12σ, while GLE 77 is more moderate and consistent across the three detectors, with peak significances from 4.57σ to 5.41σ. This difference may be due to variations in solar proton energy, anisotropy, temporal development, or atmospheric propagation, though further physical analysis beyond this statistical comparison is needed.

GLE 69 was associated with the X7.1 flare of 20 January 2005, which peaked near 7:00, coinciding with the earliest relativistic ground response. The Aragats muon measurements are especially important because the first impulse, observed near 07:02 UT, was detected in the Aragats Multidirectional Muon Monitor with a threshold of about 5 GeV. This implies primary solar protons with energies of roughly 20–30 GeV (Bostanjan et al., 2007; Chilingarian et al., 2009).

The GLE 69 was highly directional and had a very hard spectrum, with a narrowly focused relativistic component during the initial rise (Gopalswamy et al., 2012; Bieber et al., 2013). The earliest impulse corresponds to a prompt, ultrarelativistic proton release, while the later enhancements correspond to delayed, softer components. This picture is also supported by multiwavelength solar analyses, which concluded that the relativistic proton profile of 20 January 2005 contained successive releases, and that the delayed component was linked to post-impulsive magnetic restructuring in the corona rather than to a single continuous accelerator (Simnett, 2006; Klein et al., 2014).

An important difference between the two events is the spectral evolution during their development: the earliest

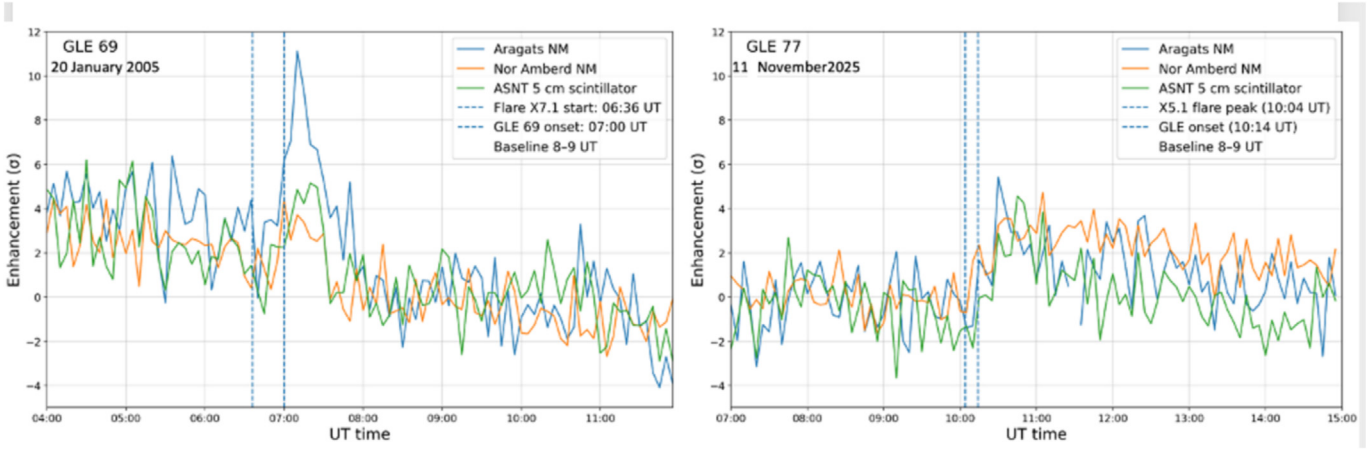

Fig. 1. GLE 69: five-minute significance time series with a baseline of 08:00–09:00 UT, flare starts at 06:36 UT, and GLE onset at ≈ 07:00 UT. GLE 77: five-minute significance time series with a baseline of 08:00–09:00 UT, flare peak at 10:04 UT, and GLE onset at 10:14 UT. For GLE 69, the 08:00–09:00 UT interval was used as the baseline because the pre-event count rate showed a broad bump in the hours preceding the onset. Using a pre-increase interval would therefore bias the significance estimate. The post-event interval was adopted as a better approximation of the underlying background level.

phase of GLE 69 contained the hardest particles, while later increases involved progressively softer populations. GLE 77 appears broader and more spread out over time. Its detector profiles suggest a less impulsive, more gradual development, which aligns with a softer or less sharply injected particle population, although additional spectral analysis would be needed for a definitive conclusion.

The detector pattern also supports this distinction. In GLE 69, the most significant physical feature is not just the amplitude of the neutron monitor increase, but the fact that muon, neutron monitor, and scintillator channels responded almost simultaneously during the earliest minutes. This combination occurs only when the initial proton spectrum reaches very high energies. In GLE 77, the responses of the available detectors are more balanced and similar in scale, but they do not show as clear a threshold-crossing signature of an ultrarelativistic primary component as in GLE 69. Therefore, GLE 69 appears to be the more energetic and physically extreme event, whereas GLE 77 was broader, less impulsive, and less clearly dominated by an ultrarelativistic primary component.

3. FD on 19–20 January 2026, registered by neutron monitors and SEVAN network

A long-duration X1.95 solar flare from active region AR 4341 reached its soft X-ray maximum at 18:09 UT on 18 January 2026. The flare was accompanied by a large coronal mass ejection whose full-halo appearance in coronagraph images confirmed a substantial Earth-directed component. The associated interplanetary disturbance reached Earth on 19 January, triggering a major geomagnetic storm. From 19 to 21 January, geomagnetic activity reached severe storm levels (G4) for approximately 15 h and remained at strong storm levels (G3) for more than 18 h. This prolonged disturbance was accompanied by unusually widespread auroral activity, indicating the storm's exceptional intensity and spatial extent. In terms of both intensity and duration, this event was one of the major space-weather disturbances of Solar Cycle 25.

Geomagnetic measurements at Aragats revealed a sharp dip in the X-component of the magnetic field, with a clear minimum at 21:26 UT on January 19. The magnetic response showed a step-like decrease, consistent with sudden magnetospheric compression followed by ring-current intensification. The timing of this magnetic minimum serves as a useful reference for the arrival of the ICME-driven shock and sheath at Earth. Immediately after the geomagnetic response, a clear FD was observed by multiple neutron monitors and the SEVAN network (Fig. 2). The decrease began within a narrow time frame, with slight station-to-station differences caused by variations in geomagnetic cutoff rigidity and viewing direction. Nor Amberd recorded the earliest onset, closely followed by Lomnický Štít, Oulu, and Apatity. The FD depth reached about 15–20% below the pre-event level, showing effective suppression of galactic cosmic rays due to the strengthened magnetic field and turbulence associated with the ICME sheath and magnetic cloud. A suppression was observed by the SEVAN network at mid-altitude stations, including Aragats, Lomnický Štít, and Musala. In the setup used here, the SEVAN "010" channel, which detects signals only in the middle scintillator, is mainly influenced by secondary neutrons with a small contribution from muons, making it broadly comparable to neutron monitor observations. The temporal profiles recorded by SEVAN display the classic FD shape seen in neutron monitors: a sudden onset, a quick transition to a reduced level, and a slower recovery. This similarity suggests that both detector systems tracked the same large-scale modulation of the secondary particle field caused by the ICME disturbance. The remaining differences are mostly quantitative: SEVAN onset times seem slightly more spread out and sometimes a bit later than those from neutron monitors, primarily because the SEVAN "010" channel has different counting statistics and a response function that is not identical to a standard neutron monitor.

The temporal ordering of the observations is consistent across the available datasets. The geomagnetic disturbance, marked by the minimum of the X-component, preceded the onset of the FD in neutron monitors, which in turn coincided with or slightly preceded the suppression observed by the SEVAN network. This sequence supports a causal chain linking the ICME-driven shock to magnetospheric compression and subsequent cosmic-ray modulation. The consistency of timing and behavior across independent measurement techniques demonstrates the diagnostic value of coordinated geomagnetic, neutron-monitor, and secondary-particle observations during extreme space-weather events.

In Fig. 3, we compare the FD measured by the ASNT with that measured by NANM. The FD amplitude recorded by the neutron monitor is significantly larger than that recorded by the ASNT muon-dominated channels.

The markedly different FD amplitudes in neutron and muon channels follow naturally from the rigidity dependence of heliospheric modulation during ICME-driven disturbances. Neutron monitors respond primarily to the nucleonic component generated by primaries with characteristic rigidities of a few to roughly 10 GV, depending on geomagnetic cutoff and atmospheric depth, whereas ground-level muons are preferentially produced by higher-rigidity primaries, typically tens of GV and above. Because the fractional suppression of galactic cosmic rays decreases with increasing rigidity, the neutron-monitor decrease is expected to be larger than the muon decrease. The present event exhibits exactly this behavior: the neutron channels show a deep suppression of order 15–20%, whereas the muon-dominated ASNT response is noticeably smaller.

In Fig. 4, we display the well-known Halloween events of 2003. The FD amplitude reaches 23% at Aragats, marking one of the most notable space weather events recorded. On October 29, 2003, a fast ICME (~2000 km/s) struck

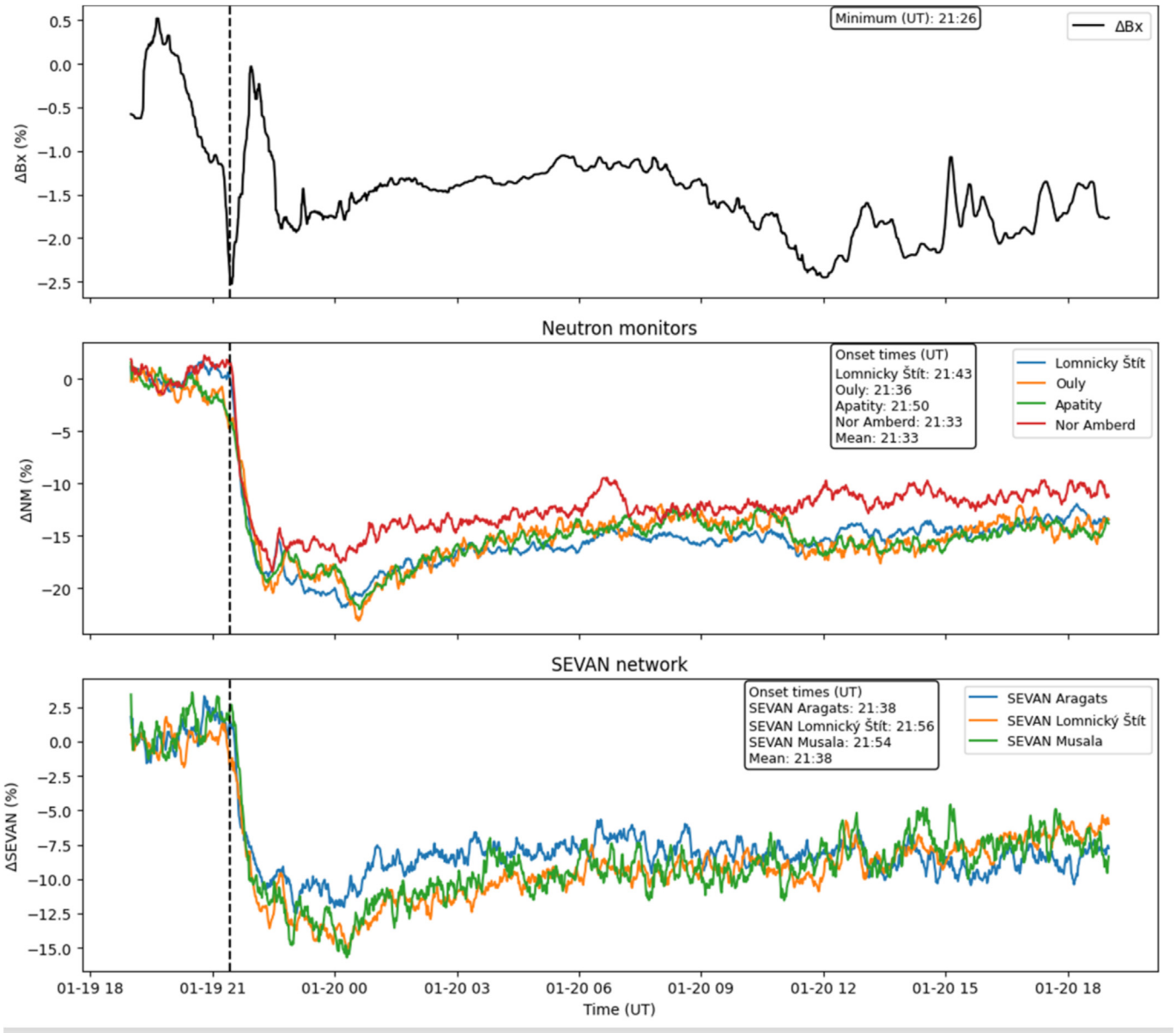

Fig. 2. Time-aligned response of the geomagnetic field, neutron monitors, and SEVAN detectors during the January 2026 FD. The top panel shows the filtered X-component of the geomagnetic field at Aragats, expressed as a percentage deviation from the pre-event baseline; the vertical dashed line marks the time of the magnetic-field minimum associated with the arrival of the ICME-driven disturbance. The middle panel presents relative count-rate variations recorded by four neutron monitors (Nor Amberd, Lomnický Štít, Oulu, and Apatity), with onset times indicated for each station. The bottom panel shows the corresponding suppression observed by the SEVAN network at Aragats, Lomnický Štít, and Musala. All data are normalized to the same baseline interval, illustrating the coherent temporal progression from geomagnetic disturbance to cosmic-ray modulation.

Earth's magnetosphere, causing a strong geomagnetic storm (Dst ~ -383 nT). Between October 29 and 30, 2003, a deep FD was observed worldwide. A second ICME from an X1.2 flare from the same active region, which peaked at 16:53 UTC on October 31, arrived at Earth at 23:00, causing a second drop that deepened the FD by approximately 5% at some stations. This historical comparison emphasizes that the January 2026 event belongs among the major space-weather disturbances of the current solar cycle.

4. Energy spectra related to FD, comparison with GLE

In this subsection, we demonstrate the capability of SEVAN Light detectors to reconstruct energy-release spectra of secondary neutral (mostly neutrons) and charged particles(mostly muons). First, we describe the method for recovering energy spectra from energy release histograms. These histograms display the number of events versus the energy released in the detector. The Logarithmic Amplitude-Digit Converter (LADC), used in MAKET and

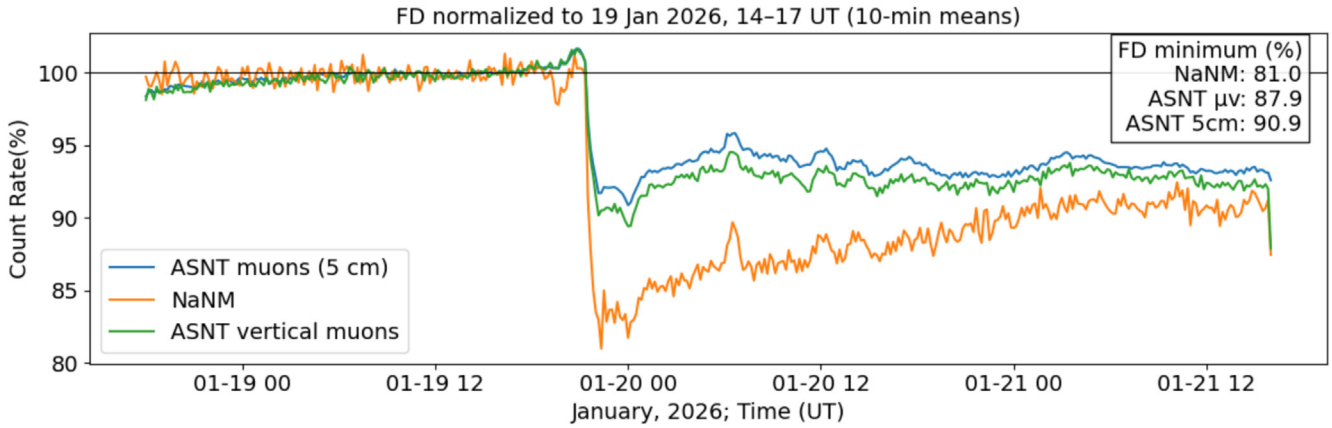

Fig. 3. Comparison of the FD recorded by NANM and by the ASNT muon-dominated channels. The neutron monitor exhibits a substantially larger FD amplitude than the ASNT channels, reflecting the stronger modulation of lower-rigidity primary cosmic rays. The temporal evolution of the disturbance is similar for neutrons and muons, indicating a common interplanetary driver. Spikes during the recovery phase are caused by gamma-ray contamination associated with a wind-driven gamma-ray storm during a major snowfall at Aragats (Chilingarian et al., 2025).

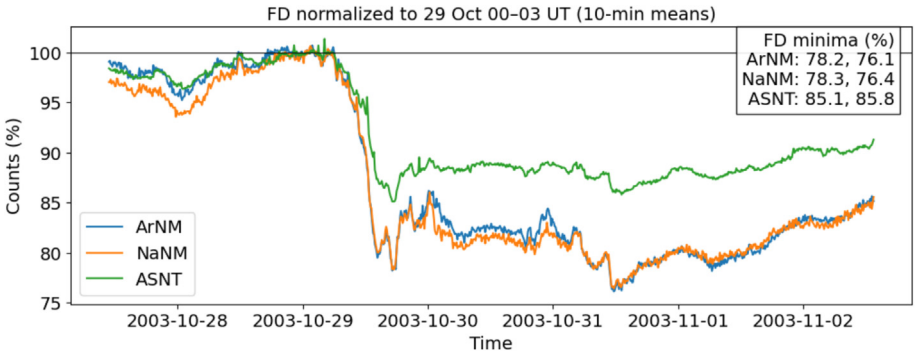

Fig. 4. The FD during the Halloween events of October–November 2003 showed that the FD amplitude measured by neutron monitors reached 24%, while the muon detector (4 m^2 area, 5 cm thick scintillator) recorded 15%. The disturbance had a two-stage structure, with a second ICME arriving before the system recovered from the first. In the inset, the amplitudes of the first and second dips are displayed. Notably, the muon count rate did not decrease following the arrival of the second ICME.

SEVAN Light electronics, has a distinctive feature that allows for the acquisition of spectra up to 50 MeV. The LADC applies a logarithmic function to the input signal, meaning that the quantization step size varies depending on the input signal's amplitude. This enables the LADC to handle a wide dynamic range of input signals by compressing higher amplitudes and expanding lower ones.

To determine the original energy spectrum from measured energy release, we solve the inverse problem. This task is complex because cosmic ray interactions and detection processes distort the original energy distribution. Estimating the detector's response function generally involves predicting outcomes for a known set of inputs (solving the direct problem). The response function describes how a detector responds to different particle fluxes at various energies, indicating the probability of measuring energy deposit E_{dep} if the true energy is E_{true}. Particle fluxes at any geographic coordinates and altitudes were obtained from the EXPACS web calculator (Sato, 2016). The GEANT4 code (Agostinelli et al., 2003) was used to simulate particle transport through different media, accounting for various sources of randomness and measurement uncertainties. Consequently, the response matrix includes the smearing effects caused by the detector's finite resolution and the asymmetry in bin-to-bin migration due to steep cosmic ray spectra. The energy release in the detector simulated with GEANT4 was converted into LADC codes using the following expression:

$$[k] = d \cdot ln\frac{E_{dep}}{E_0} + k_0 \quad (1)$$

where $[k] \geq 1$ is the LADC code, $d \approx 10.5$ is the LADC scale factor, E_{dep} is the energy release in the scintillator, E_0 is the average muon energy release in the plastic scintillator, and k_0 is the LADC code corresponding to the energy loss of a minimum-ionizing particle (MIP) in the detector.

As a result of simulation trials, we obtain the response matrix A_{ij}, which shows how simulated particles with input energy x_i (i = 1, N) are distributed across bins y_j (the number of simulated events falling into energy bin I after processing by the detector response). Therefore, the response matrix $A_{i,j}$ indicates the likelihood that an event with true (simulated) energy in bin i will be registered in bin j.

$$y_j = \sum_{i=1}^{N} A_{ij} x_i, i = 1, ..., N. \quad (2)$$

The energy deposit E_{dep} (MeV) was simulated for a given set of energies E_j (j = 1, N) spanning an energy range from 1 to 300 covered by N = 127 energy bins. Conversion of energy to LADC codes was performed according to Eq. (1). M = 10^5 events were simulated for each E_j. The response matrix was normalized by the total number of simulation trials (M × N). During the matrix calculation, we considered particle registration efficiency, which varies by particle type and energy. To retrieve the actual energy spectrum from the measured energy deposit histogram, we applied an unfolding procedure based on inversion of the detector response matrix A, to ultimately obtain the energy spectrum.

$$x_i = \sum_{j=1}^{N} (A^{-1})_{ij} y_j, i = 1, ..., N. \quad (3)$$

The derived energy spectra are validated with different detectors and observational methods. The count rates of the SEVAN Light detector were estimated using the recovered energy spectrum of a large TGE that occurred on October 6, 2021. The experimentally observed and simulated particle fluxes at the peak of TGE development agreed to within approximately 20% (Chilingarian et al., 2022a; see Table 2 of Chilingarian et al., 2022b). The TGE spectra were recovered by various spectrometers, including a large 4 m^2 area and 60 cm thick ASNT scintillation spectrometer (Chilingarian et al., 2022c), large (12 × 12 × 30 cm) NaI (Tl) spectrometers (Chilingarian et al., 2015), and CUBE scintillation spectrometers. In Fig. 12 of (Chilingarian et al., 2023a), the differential energy spectra of a large TGE on October 6, 2021, were compared, and all three reconstructed energy spectra agree reasonably well. The obtained differential energy spectra of gamma rays and electrons were approximated using a five-parameter fit, including the spectral knee position (Chilingarian et al., 2023b).

For FDs, the same instrumental capability can be used in a reverse but physically meaningful way. Instead of excess particles, FDs are characterized by a deficit of cosmic rays compared to a quiet-time reference state before the interplanetary disturbance. Using SEVAN Light data, one can define "missing-particle spectra" as the difference between the quiet-time secondary-particle spectra and those measured during the main phase of the FD. These spectra quantify, as a function of secondary energy, which particles are removed from the flux during the ICME–magnetosphere interaction.

The concept of missing-particle spectra is useful because it maintains information on energy dependence that is lost in integral count-rate measurements. Although neutron monitors provide high-precision records of intensity reductions, their response sums over a broad range of primary rigidities, making it hard to determine whether the suppression is mainly caused by lower-rigidity particles or extends evenly to higher rigidities. Simultaneous reconstruction of neutron and muon deficit spectra thus allows a comparative analysis of the missing particle populations associated with different primary-rigidity ranges.

Neutrons mainly reflect the modulation of lower-rigidity primary cosmic rays, while muons probe higher rigidities because of the kinematics of pion production and decay in the atmosphere. Therefore, differences in the depth, spectral shape, and temporal evolution of neutron and muon deficits directly reveal the rigidity dependence of the FD. A stronger suppression of neutron spectra relative to muons indicates more efficient removal of lower-rigidity particles, often associated with increased magnetic turbulence in the ICME sheath. The different behaviors of neutron and muon channels can thus be explained by their different rigidity responses, with neutron monitors being more sensitive to lower-rigidity primaries and muon detectors sampling a harder part of the spectrum (Alania et al., 2013).

The link between missing-particle spectra and geomagnetic disturbances becomes especially significant during intense events such as January 19–21, 2026, when extended G4–G3 conditions indicate a strong coupling between the interplanetary magnetic field and Earth's magnetosphere. During these periods, magnetospheric compression, changes in cutoff rigidity, interplanetary scattering, and adiabatic deceleration can alter the spectrum observed at Earth, particularly at lower rigidities (Ruffolo, 1995; Qin et al., 2004). In this context, missing-particle spectra serve as a quantitative tool to assess how different rigidity ranges of cosmic rays are suppressed during combined interplanetary and magnetospheric disturbances. Geomagnetic storm severity is formally characterized by indices such as Kp, Ap, and Dst, which measure disturbances in the geomagnetic field independently of particle-flux data. Therefore, SEVAN Light observations do not directly measure storm intensity in the conventional geomagnetic sense. Instead, their importance lies in characterizing the rigidity-dependent modulation of cosmic rays caused by interplanetary disturbances and their interaction with the magnetosphere. When analyzed alongside standard geomagnetic indices, these spectral deficits provide complementary insights into how ICME-driven magnetic structures influence particle access to the atmosphere during geomagnetic storms.

Fig. 5 presents the relative integral spectra of missing neutral particles (mainly neutrons) and charged particles (primarily muons) during the FD interval, normalized to the intensities at 10 MeV to highlight differences in spectral shape. The figure illustrates the temporary suppression of GCRs by interplanetary magnetic structures. This suppression depends on energy, showing a stronger effect at lower rigidities and a gradual reduction of the neutron deficit at higher energies. The muon spectrum is less impacted than the neutron spectrum, aligning with the fact that muons

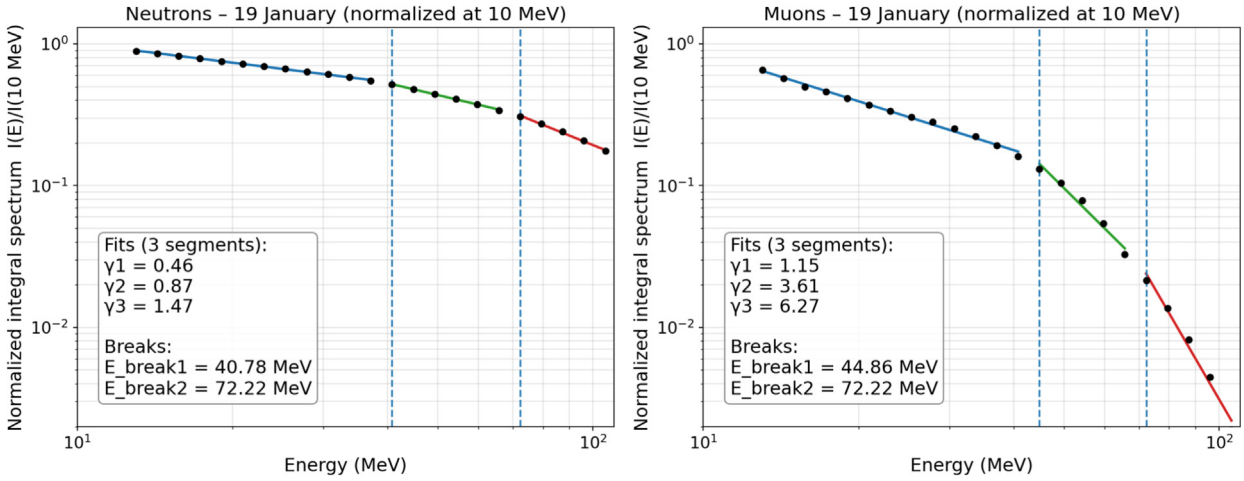

Fig. 5. Relative integral energy spectra of "missing" neutral particles (mostly neutrons) and charged particles (mostly muons) during FD, normalized to the intensities at 10 MeV.

are mainly produced by higher-energy primaries that are less affected by GCR modulation.

The FD amplitude is larger for neutrons than for muons at all energies, in agreement with Fig. 3. Neutrons detected at ground level are produced predominantly by lower-energy primary protons near the geomagnetic cutoff and within the rigidity range most strongly modulated by interplanetary magnetic structures. Muons are produced by higher-energy primaries because pion production and decay require substantially higher primary energies and deeper shower development. Since FD suppresses the GCR flux most efficiently at low rigidities, the neutron component experiences a stronger reduction, whereas the muon component, fed by higher-rigidity primaries, is less affected.

The neutron deficit spectrum shows a relatively flat low-energy segment, followed by moderate steepening above the first break and stronger steepening at higher energies. This structure is consistent with a mixed contribution from primaries near the cutoff rigidity, competition between hadronic production and atmospheric attenuation, and a progressive weakening of FD influence with increasing primary rigidity. In contrast, the fitted muon spectrum is steeper across all segments, with the highest-energy segment steepening much more rapidly than in the neutron case (6.27 versus 1.47). This behavior reflects the fact that muons sample a narrower, higher-energy primary population, where FD modulation is already weaker.

Fig. 6 compares the integral spectra obtained with SEVAN Light during the GLE and during the FD deficit,

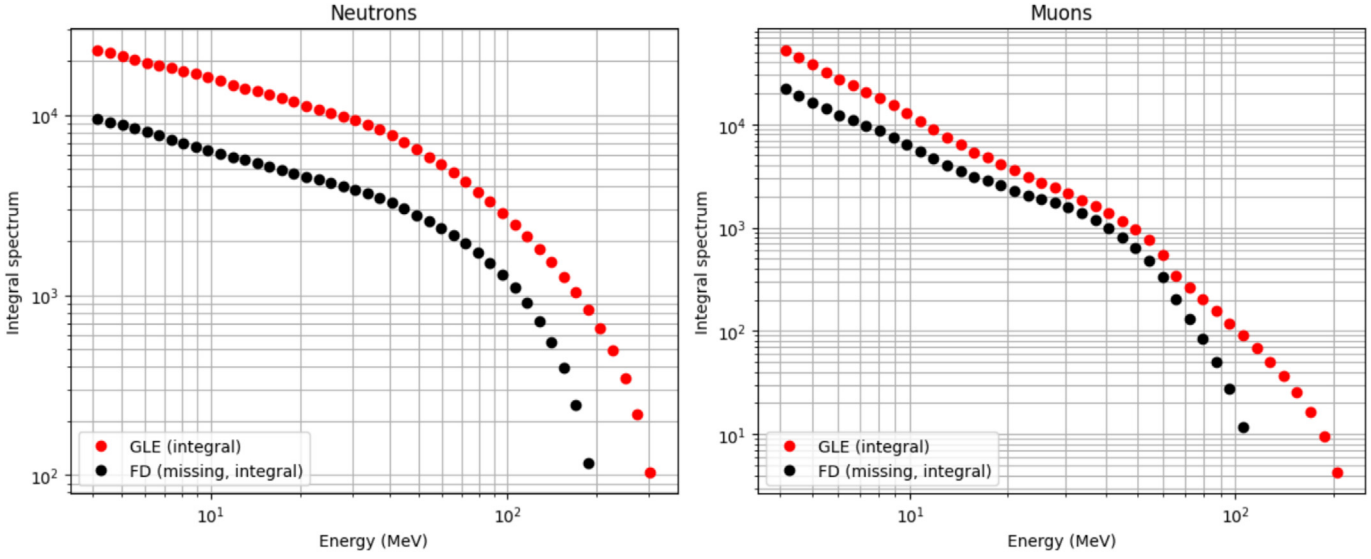

Fig. 6. Integral energy spectra of neutrons (left) and muons (right) during the GLE and FD are plotted together starting from 10 MeV. The FD spectra represent the energy-dependent deficit ("missing" particles) relative to background GCR conditions, while the GLE spectra show the enhancement caused by solar energetic protons. This comparison highlights the inherent asymmetry between suppression and injection processes, as well as the different responses of the neutron and muon channels.

shown separately for neutrons and muons. The GLE energy spectrum was reconstructed using Eqs. (1)–(3), after subtraction of the pre-event background. The comparison shows that neutrons and muons respond very differently at the high-energy end of the spectrum. In both panels, the GLE enhancement remains substantial at higher deposited energies, whereas the FD deficit steepens and becomes relatively weaker. This divergence is more pronounced in the muon channel than in the neutron channel. In practical terms, the high-energy tail is much more robust for muons in the GLE than in the FD deficit, consistent with the fact that ground-level muons preferentially sample higher-energy primaries and are therefore especially sensitive to the presence or absence of a multi-GeV component, whereas the neutron response is fed efficiently by a broader and generally lower primary-energy range.

5. Conclusion

The FD of January 19–20, 2026, was clearly detected by both the global neutron-monitor network and the SEVAN detector system, demonstrating consistent cosmic-ray modulation across independent instruments and particle populations. Neutron monitors showed a stronger suppression than the muon-dominated SEVAN channels, confirming that lower-rigidity galactic cosmic rays were affected more strongly than the higher-rigidity primaries responsible for ground-level muons.

The reconstructed "missing-particle" spectra preserve information on energy dependence that is lost in integral count-rate measurements. They show that the FD deficit is systematically larger in the neutron component than in the muon component at all measured energies, and that the muon deficit weakens more rapidly toward high energies. In contrast, GLE spectra retain a substantial high-energy tail, especially in the muon channel. This comparison reveals a fundamental asymmetry between the suppression of galactic cosmic rays during FDs and the injection of solar particles during GLEs.

These results show that the joint use of neutron monitors and SEVAN spectrometry provides a powerful method for studying rigidity-dependent cosmic-ray modulation during extreme solar events. Neutron monitors define the timing and amplitude of the global decrease, while SEVAN adds energy-resolved separation of neutron- and muon-dominated responses. Together, they provide a more complete picture of how ICME-driven disturbances and SEP events modify particle access to the atmosphere.

Data availability

The neutron and muon data from the ASNT and the SEVAN Light detector that support the findings of this study are available from the corresponding author upon reasonable request. Processed data products and reconstructed spectra used in this analysis are derived from these measurements using standard procedures described in the manuscript. GOES proton data are publicly available from NOAA archives.

Declaration of competing interest

The authors declare that they have no known competing financial interests or personal relationships that could have appeared to influence the work reported in this paper.

Acknowledgement

The authors acknowledge the support of the Science Committee of the Republic of Armenia (Research Project No. 21AG-1C012).

References

Agostinelli, S. et al., 2003. GEANT4 - a simulation toolkit. Nucl. Instrum. Methods Phys. Res., Sect. A 506 (3), 250–303. https://doi.org/10.1016/S0168-9002(03)01368-8.

Alania, M.V., Wawrzynczak, A., Sdobnov, V.E., Kravtsova, M.V., 2013. Temporal changes in the rigidity spectrum of Forbush decreases based on neutron monitor data. Sol. Phys. 286, 561–576. https://doi.org/10.1007/s11207-013-0273-0.

Bieber, J.W., Clem, J., Evenson, P., Pyle, R., Sáiz, A., Ruffolo, D., 2013. Giant ground level enhancement of relativistic solar protons on 2005 January 20. I. Spaceship Earth observations. Astrophys. J. 771 (2), 92. https://doi.org/10.1088/0004-637X/771/2/92.

Bostanjan, N., Chilingarian, A., Eganov, V., Karapetyan, G., 2007. On the production of the highest-energy solar protons on 20 January 2005. Adv. Space Res. https://doi.org/10.1016/j.asr.2007.03.024.

Bütikofer, R., Flückiger, E.O., 2015. What are the causes for the spread of GLE parameters deduced from NM data? J. Phys. Conf. Ser. 632 (1), 012053. https://doi.org/10.1088/1742-6596/632/1/012053.

Chilingarian, A., 2009. Statistical study of the detection of solar protons of the highest energies on 20 January 2005. Adv. Space Res. 43, 702–707. https://doi.org/10.1016/j.asr.2008.10.005.

Chilingarian, A., Babayan, V., Karapetyan, T., et al., 2018. The SEVAN Worldwide network of particle detectors: 10 years of operation. Adv. Space Res. 61, 2680. https://doi.org/10.1016/j.asr.2018.02.030.

Chilingarian, A., Chilingaryan, S., Hovsepyan, G., 2015. Calibration of particle detectors for secondary cosmic rays using gamma-ray beams from thunderclouds. Astropart. Phys. 69, 37–43. https://doi.org/10.1016/j.astropartphys.2015.03.011.

Chilingarian, A., Hovsepyan, G., Karapetyan, T., Sargsyan, B., Chilingaryan, S., 2022a. Measurements of energy spectra of relativistic electrons and gamma-rays from avalanches developed in the thunderous atmosphere with Aragats Solar Neutron Telescope. J. Instrum. 17, P03002. https://doi.org/10.1088/1748-0221/17/03/P03002.

Chilingarian, A., Hovsepyan, G., Karapetyan, T., Khanykyanc, Y., Pokhsraryan, D., Sargsyan, B., Chilingaryan, S., Soghomonyan, S., 2022b. Multi-messenger observations of thunderstorm-related bursts of cosmic rays. J. Instrum. 17, P07022. https://doi.org/10.1088/1748-0221/17/07/P07022.

Chilingarian, A., Hovsepyan, G., Karapetyan, T., Kozliner, L., Chilingaryan, S., Pokhsraryan, D., Sargsyan, B., 2022c. 'The horizontal profile of the atmospheric electric fields as measured during thunderstorms by the network of NaI spectrometers located on the slopes of Mt. Aragats'. J. Instrum. 17, P10011. https://doi.org/10.1088/1748-0221/17/10/P10011.

Chilingarian, A., Hovsepyan, G., Aslanyan, D., et al., 2023a. Thunderstorm ground enhancements observed on Aragats Mountain in Armenia in the wintertime. EPL (Europhysics Lett.) 143, 59002. https://doi.org/10.1209/0295-5075/acf340.

Chilingarian, A., Hovsepyan, G., Karapetyan, T., Aslanyan, D., Chilingaryan, S., Sargsyan, B., 2023b. Genesis of thunderstorm ground enhancements. Phys. Rev. D 107, 102003. https://doi.org/10.1103/PhysRevD.107.102003.

Chilingarian, A., Karapetyan, T., Sargsyan, B., Knapp, J., Walter, M., Rehm, T., 2024. Energy spectra of the first TGE observed on Zugspitze by the SEVAN light detector compared with the energetic TGE observed on Aragats. Astropart. Phys. 156, 102924. https://doi.org/10.1016/j.astropartphys.2024.102924.

Chilingarian, A., Sargsyan, B., Aslanyan, D., Kozliner, L., 2025. Wind-induced natural gamma radiation. EPL (Europhysics Letters) 151, 14001. https://doi.org/10.1209/0295-5075/ade562.

Forbush, S.E., 1954. World-wide cosmic-ray variations in 1937-1952. J. Geophys. Res. 59, 525. https://doi.org/10.1029/JZ059i004p00525.

Gopalswamy, N., Xie, H., Akiyama, S., Mäkelä, P., Yashiro, S., 2012. Properties of ground level enhancement events and the associated solar eruptions during solar cycle 23. Space Sci. Rev. 171, 23–60. https://doi.org/10.1007/s11214-012-9890-4.

Klein, K.-L., Masson, S., Bouratzis, C., Grechnev, V., Hillaris, A., Preka-Papadema, P., 2014. The relativistic solar particle event of 2005 January 20: origin of delayed particle acceleration. Astron. Astrophys. 572, A4. https://doi.org/10.1051/0004-6361/201423783.

Kress, B.T., Rodriguez, J.V. and Onsager, T.G. 2020, 'The GOES-R Space Environment In Situ Suite (SEISS): Measurement of Energetic Particles in Geospace'. In: Goodman, S.J., Schmit, T.J., Daniels, J. and Redmon, R.J. (Eds.), The GOES-R Series. Elsevier. pp. 243-250. doi: 10.1016/B978-0-12-814327-8.00020-2.

Maricic, D., Vrsnak, B., Dumbovic, M., et al., 2014. Kinematics of interacting ICMEs and related Forbush decrease: case study. Sol. Phys. 289, 351–368. https://doi.org/10.1007/s11207-013-0314-8.

Mishev, A.L., Usoskin, I.G., 2016. Analysis of the ground level enhancements on 14 July 2000 and on 13 December 2006 using neutron monitor data. Sol. Phys. 291 (4), 1225–1239. https://doi.org/10.1007/s11207-016-0877-2.

Qin, G., Zhang, M., Dwyer, J.R., Rassoul, H.K., 2004. Interplanetary transport mechanisms of solar energetic particles. Astrophys. J. 609 (2), 1076–1081. https://doi.org/10.1086/421101.

Reames, D.V., 2013. The two sources of solar energetic particles. Space Sci. Rev. 175, 53–92. https://doi.org/10.1007/s11214-013-9958-9.

Ruffolo, D., 1995. Effect of adiabatic deceleration on the focused transport of solar cosmic rays. Astrophys. J. 442, 861–874. https://doi.org/10.1086/175489.

Sato, T., 2016. Analytical model for estimating the zenith angle dependence of terrestrial cosmic-ray fluxes. PLoS One 11, e0160390. https://doi.org/10.1371/journal.pone.0160390.

Shea, M.A., Smart, D.F., 2012. Space weather and the ground-level solar proton events of 23rd solar cycle. Space Sci. Rev. 171, 161–188. https://doi.org/10.1007/s11214-012-9923-z.

Simnett, G.M., 2006. The timing of relativistic proton acceleration in the 20 January 2005 flare. Astron. Astrophys. 445, 715–724. https://doi.org/10.1051/0004-6361:20053503.

Tylka, A.J., Dietrich, W.F., 2009. A new and comprehensive analysis of proton spectra in ground-level enhanced (GLE) solar particle events. Proceedings of the 31st International Cosmic Ray Conference, Łódź, paper SH3.